Int j simul model 24 (2025) 2, 309-320
Original scientific paper

THERMAL SIMULATION OF UAV LI-PO BATTERIES UNDER ABNORMAL AGEING CONDITIONS

Niu, L. Q.; Wang, Y. F.; Li, Z.[#]; Miao, W. Y. & Li, X. R.
School of Civil Aviation, Zhengzhou University of Aeronautics, Zhengzhou, 450046, China
E-Mail: lizhen@zua.edu.cn ([#] Corresponding author)

Abstract
The temperature changes under thermal, electrical and mechanical abuse conditions were simulated via COMSOL Multiphysics software on the basis of heat generation mechanisms and heat transfer processes to simulate the thermal behaviour of lithium-polymer (Li-Po) batteries for unmanned aerial vehicles (UAVs). The temperature changes of batteries under different abnormal ageing conditions were analysed, the temporal–spatial evolution patterns of temperature fields were revealed, and the dynamic evolution characteristics of thermal behaviour were obtained. Results show that the maximum temperature rise of batteries after charge–discharge cycles progressively intensifies as ambient temperature increases. Overcharging and nail puncture generate substantial heat, thereby inducing abrupt temperature surges in batteries, with peak temperatures of overcharged and punctured batteries reaching 105 °C and 300 °C, respectively. The obtained conclusions provide some theoretical references and decision-making foundations for controlling thermal runaway in lithium batteries under abnormal ageing conditions.
(Received in March 2025, accepted in May 2025. This paper was with the authors 1 month for 2 revisions.)

Key Words: Abnormal Ageing, UAV Li-Po Batteries, Thermal Simulation

1. INTRODUCTION

The low-altitude economy emerges as a new engine of growth for the global economy, with civil unmanned aerial vehicles (UAVs) serving as pioneers in this domain. As the primary power source for stable flight endurance and safety-critical attitude control, UAV batteries represent a core limiting factor in expanding their applications. Lithium-polymer (Li-Po) batteries, favoured for their high energy density, long cycle life, lightweight design and environmental friendliness, dominate as the mainstream power source for UAVs. However, safety issues such as thermal runaway caused by thermal shocks, external mechanical loads and other factors during operation remain prominent. Unlike conventional consumer-grade lithium batteries, Li-Po batteries encounter problems such as high multicondition coupling and large temperature gradients because of the complex and variable service environment. These factors lead to frequent abnormal ageing conditions under harsh environmental temperatures, sudden vibration impacts and improper usage. Internal short circuits and irreversible cliff-like performance degradation problems occur more significantly in UAV Li-Po batteries than in conventional consumer-grade batteries. In extreme cases, thermal runaway occurs, directly affecting the flight safety of UAVs.

Abnormal ageing refers to the accelerated performance decline of batteries due to external factors, improper usage or internal defects. This process is often accompanied by safety hazards or irreversible damage. It generally includes thermal abuse, electrical abuse and mechanical abuse [1]. Thermal abuse occurs when batteries are used in environments beyond the designed temperature range (high or low temperatures), thereby leading to imbalances in internal chemical reactions. Electrical abuse arises from electrical operations exceeding safety limits (e.g. overcharging and over-discharging), thereby causing internal structural damage. Mechanical abuse involves external forces that can deform batteries, thereby triggering internal short circuits, electrolyte leakage or thermal runaway. Thermal runaway is a direct manifestation of advanced abnormal ageing. Investigating the thermal behaviour of batteries under abnormal ageing conditions is essential for ensuring intrinsic safety. Current research on the thermal behaviour of lithium batteries mainly focuses on thermal runaway caused by a single abnormal ageing condition [2-4]; however, limited attention is given to scenarios where multiple abuse conditions coexist. In practical applications, abnormal ageing conditions, such as thermal abuse, electrical abuse and mechanical abuse, affect lithium batteries, thereby posing a systemic risk chain to the safety performance of lithium batteries. Systematically exploring the thermal behaviour of batteries under different abnormal ageing conditions is a prerequisite for exploring the risk chains of thermal runaways caused by different abnormal ageing conditions [5]. Most studies of UAV lithium batteries employ experimental methods to analyse collision safety under mechanical abuse [6, 7], with few investigations being conducted on thermal or electrical abuse. Impact tests involving violent compression pose combustion or explosion risks, resulting in high costs, low repeatability and insufficient data for follow-up research. The thermal behaviour of UAV Li-Po batteries under thermal abuse, electrical abuse and mechanical abuse scenarios was designed to address the above deficiencies, and the temperature evolution at different time steps was compared using the technical method of simulation to reveal the thermal runaway characteristics under different abnormal ageing conditions. Furthermore, the key spatial–temporal points of thermal behaviour were proposed to control temperature rise and improve the safety management level of UAV Li-Po batteries comprehensively.

2. STATE OF THE ART

In the research field of lithium battery thermal behaviour, related research focuses on performance degradation and thermal runaway under a single abnormal ageing condition, with limited exploration of combined effects from multiple abuse conditions being conducted. For instance, Finegan et al. [8] simulated mechanical abuse in 18650 lithium batteries through puncture tests, and internal structural degradation and temperature mechanisms were characterised at different penetration positions and orientations by using infrared imaging and thermocouples. Bai et al. [9] induced internal short circuits in electric vehicle lithium batteries via hemispherical indentation tests at varying temperatures to investigate deformation and fracture patterns. Liu et al. [10] applied incremental capacity analysis and electrochemical impedance spectroscopy to study the ageing behaviour and thermal stability of 18650 lithium batteries under light overcharging cycles. Ren et al. [11] designed the liquid-nitrogen-ceased thermal runaway test to explore the relationship between internal short circuits and thermal runaway under thermal abuse. Systematic research on multiple abuse conditions has gradually attracted attention as the causes of thermal runaways continue to be explored deeply. Christensen et al. [12] monitored the thermal runaway process of lithium nickel manganese cobalt oxide batteries under thermal and mechanical abuse by using optical/thermal cameras, thermocouples and voltage measurements. Dong et al. [13] established an experimental system for three abuse conditions: acupuncture, overheating and overcharging; moreover, the effects of different abuse conditions on the surface temperature, internal temperature and battery voltage of ternary lithium batteries were compared and analysed. From the above research results, relevant scholars mainly conducted extensive experimental tests on diverse battery samples, ageing scenarios and abuse combinations. Sensing measurement devices were used to obtain physical parameters of thermal runaway and heat propagation, thereby providing indispensable empirical data and direct safety verification for lithium battery thermal behaviour research. However, experimental approaches face limitations in reliance on high-precision equipment, explosion risks during testing and discontinuous data acquisition across multiple conditions. Therefore, systematic investigations into the temporal evolution of thermal states under multiple abnormal ageing conditions become constrained by laboratory methods and remain scarce.

Furthermore, researchers in the field of numerical simulation for lithium batteries mainly focus on material design, performance parameter prediction and thermal behaviour modelling. Franco's research team [14, 15] employed coarse-grained molecular dynamics simulations to simulate the electrode preparation process, and COMSOL was utilised to simulate the electrochemical behaviour of electrode mesostructures during the battery discharge. Soltani et al. [16] applied a data-driven feedforward neural network to predict the life of lithium titanate batteries based on capacity degradation trends. The initial thermal behaviour simulation models for lithium batteries were constructed on electrochemical mechanisms. The pseudo-two-dimensional (P2D) model based on electrochemical mechanisms developed by Fuller et al. [17], known for its high accuracy, has been widely adapted and modified in thermal runaway models. Battery thermal behaviour involves a complex multiphysics system strongly coupled with mechanical, thermal and electrical fields. Multiphysics-coupled modelling has become the mainstream approach for simulating lithium battery thermal behaviour under abuse conditions, thereby aligning it with actual thermal runaway mechanisms. Lee and Kim [18] proposed a bidirectional nonlinear mechanical–electrochemical–thermal coupling method to analyse internal short circuits induced by quasi-static indentation and predict voltage drops and temperature rises. Fang et al. [19] developed 3D electrochemical–thermal coupling models under two internal short circuit modes to investigate battery electrothermal responses. Kwak et al. [20] established a multiphysics thermal runaway model for lithium iron phosphate batteries to characterise thermal runaway paths under electrical and thermal abuse. In summary, numerical simulation techniques enable dynamic exploration of internal battery changes under diverse ageing conditions. They also provide comprehensive performance parameters and thermal behaviour information, thereby serving as an effective method for quantifying microscopic reaction processes. Regarding the numerical simulation of lithium battery thermal behaviour, the research on lithium battery thermal behaviour simulations predominantly focuses on one or two abuse conditions; thus, systematic modelling of combined effects from all three abnormal ageing factors remains lacking. Additionally, the research perspectives often emphasise overall temperature trends or performance parameter curves under specific conditions [21]; however, real-time 3D visualisation of temperature evolution across battery components remains limited. These limitations hinder the practical application of thermal behaviour simulation models in engineering and restrict their theoretical support for thermal management in UAV lithium batteries.

Therefore, in light of the deficiencies in the extant studies, this study established an electro-chemical–thermal coupled model for Li-Po batteries by integrating electrochemical reactions, heat generation mechanisms and thermal exchange processes. The model incorporated factors such as charge–discharge cycles, short-circuit simulations and solid heat transfer. It considered Ohmic polarisation heat and reversible and irreversible heat from electrochemical reactions. Moreover, global methods were employed to simplify calculations of the average temperature and heat sources, whereas local methods were used to calculate spatial temperature and heat source distributions. This study investigated thermal distribution and evolution in Li-Po batteries under various abnormal ageing conditions to manage systematically the thermal runaway in UAV Li-Po batteries under such scenarios. The findings can provide theoretical insights to enhance the safety of UAV Li-Po batteries.

3. METHODOLOGY

3.1 Thermal behaviour simulation

COMSOL Multiphysics was derived from MATLAB's Toolbox module and combined with the multiphysics coupling advantage. In addition, COMSOL can be used to simulate 1D, 2D and 3D heat generation processes of Li-Po batteries directly; in particular, the internal resistance during battery reactions is described through Ohm's law, the temporal trends in heat generation are simulated, a simplified single-particle model and temperature equation are defined, and the heat transfer process under varying conditions is explored. In this study, COMSOL Multiphysics was used to achieve the thermal behaviour of Li-Po batteries under abnormal ageing conditions.

3.2 Physical model

In this study, the Li-Po battery model (type 883572) with a rated voltage of 3.7 V and a rated capacity of 1100 mAh was selected. $LiCoO_2$ and graphite were considered cathode and anode, respectively. The electrolyte material was composed of $LiPF_6$ in the EC:EMC solvent at a ratio of 3:7. As shown in Fig. 1 a, a battery cell model was established to simulate thermal behaviour under abnormal ageing conditions whilst simplifying calculations. The heat generated was calculated from the battery cell model and applied as thermal events to the single-particle model (Figs. 1 b and 1 c). Coupled heat sources were used to analyse the temporal evolution of the battery's overall temperature. The geometric model was meshed, as shown in Fig. 2. For the battery cell, meshing was calibrated to general physics mode with normal element size parameters [22]. Free triangular meshing was applied to boundaries, and tetrahedral meshes were generated via boundary layer inflation. The final mesh comprised 47,614 domain elements and 1,640 boundary elements. For the entire battery, meshing was also calibrated to general physics mode but with fine element size parameters. Free tetrahedral meshing yielded 3,102 domain elements and 408 boundary elements. The same general physics mode and fine parameters were used for the entire battery with a puncture zone, thereby resulting in 5,218 domain elements and 476 boundary elements.

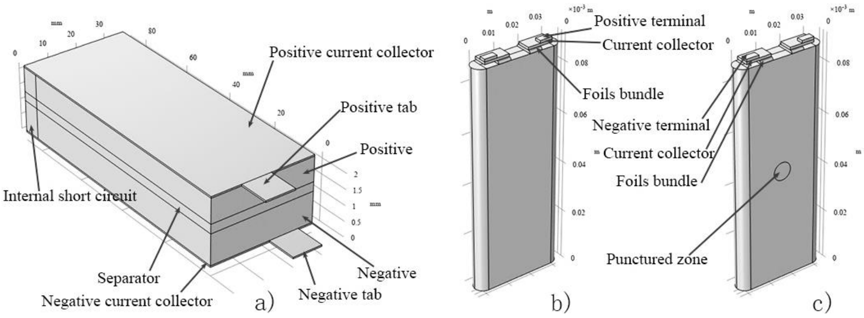

Figure 1: Schematic of the Li-Po battery geometric structure: a) battery cell geometric structure, scaled 10× in the z-direction, b) battery geometric structure, c) punctured battery geometric structure.

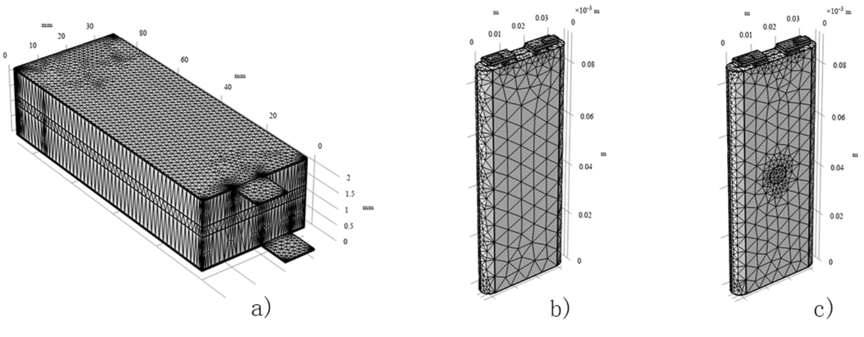

Figure 2: Schematic of the Li-Po battery meshing: a) battery cell meshing, scaled 10× in the z-direction, b) battery meshing and c) punctured battery meshing.

3.3 Mathematical model

Driven by the concentration gradient, the diffusion of active particles within the spherical particles of the electrode active material is governed by Fick's law for mass balance:

$$\frac{\partial c_s}{\partial t} = \frac{1}{r^2}\frac{\partial}{\partial r}\left(D_s r^2 \frac{\partial c_s}{\partial r}\right) \tag{1}$$

where c_s denotes the concentration of solid-phase active particles in the porous electrode, D_s represents the diffusion coefficient of the solid-phase active particles in the porous electrode, and r is the particle radius.

The conservation equation for active particles in the liquid phase of the porous electrode and separator is as follows:

$$\frac{\partial}{\partial t}\left(\psi_e c_e\right) = \nabla\left(D_{e,eff}\nabla c_e\right) + \left(1 - t_+\right)\frac{j^i}{F} \tag{2}$$

where ψ_e is the liquid-phase volume fraction of the porous electrode, $D_{e,eff}$ is the effective diffusion coefficient of the liquid phase, c_e is the liquid-phase active particle concentration in the porous electrode, t_+ is the transference number of active particles, j^i is the current density of the porous electrode, and F is Faraday constant.

The heat components most closely related to battery temperature rise are polarization heat (Q_p), Ohmic heat (Q_j), and side reactions heat (Q_{rxn}). The average internal heat generation contributing to temperature rise is expressed as:

$$Q_{total} = Q_p + Q_j + Q_{rxn} \tag{3}$$

$$Q_p = Faj^i T\frac{\partial U}{\partial T} \tag{4}$$

$$Q_j = \sigma_{s,eff}\left(\frac{\partial \phi_s}{\partial x}\right)^2 + \sigma_{e,eff}\left(\frac{\partial \phi_l}{\partial x}\right)^2 + \frac{2RT\sigma_e}{F}\left(1 - t_+\right)\left(\frac{\partial \ln c_e}{\partial x}\right)\left(\frac{\partial \phi_l}{\partial x}\right) \tag{5}$$

$$Q_{rxn} = Faj^i\left(\phi_s - \phi_e - U\right) \tag{6}$$

where $\sigma_{s,eff}$ is the solid phase effective electronic conductivity, $\sigma_{e,eff}$ is the effective ionic conductivity of the liquid phase, a is the specific surface area of the battery, ϕ_s is the electric potential of the solid phase, ϕ_l is the electric potential of the liquid phase, R is universal gas constant, T is battery temperature and U is thermodynamic equilibrium potential.

The temperature variation in the battery follows the energy conservation equation and Fourier's law:

$$\rho C_p \frac{\partial T}{\partial t} = \lambda_x \frac{\partial^2 T}{\partial x^2} + \lambda_y \frac{\partial^2 T}{\partial y^2} + \lambda_z \frac{\partial^2 T}{\partial z^2} + Q_{total} \tag{7}$$

where ρ is battery density, C_p is battery heat capacity, and λ_x, λ_y, λ_z represent thermal conductivity coefficients along the length, width, and height directions of the battery, respectively.

4. RESULTS ANALYSIS AND DISCUSSION

4.1 Thermal abuse

During the Li-Po battery operation, heat generation occurs because of internal resistance. The relationship between heat generation and dissipation rates determines the degree of heat accumulation. If the heat generation rate exceeds the dissipation rate, then the heat accumulation initiates localised overheating. This outcome may escalate into thermal runaway, thereby ultimately jeopardising battery safety. Charge–discharge cycles at a 4C rate were simulated to analyse the overall temperature variations of the battery under environmental temperatures (T) of 0, 20 and 40 °C. The results are illustrated in Figs. 3 to 5. During the charge–discharge cycles, the battery temperature increased across all environmental conditions, indicating that the heat generation rate consistently surpassed the dissipation rate. The simulations revealed high temperatures near the battery's positive and negative terminals. This arises from the proximity to current collectors, where the electrochemical activity is high, resulting in elevated heat generation rates. At $T = 0$ °C, the maximum temperature rise reached

4.0 °C (Fig. 3). At $T = 20\,°C$, the maximum temperature rise increased to 4.2 °C (Fig. 4). At $T = 40\,°C$, the maximum temperature rise peaked at 4.5 °C (Fig. 5). As the environmental temperature increased, the postcycling temperature rise also escalated. On the one hand, the reaction rate inside the battery increased with the increase in the environment temperature. On the other hand, the thermal conductivity of the battery material decreased with the increase in the environment temperature. This scenario leads to diminished heat dissipation efficiency under constant temperature gradients and heat transfer zones.

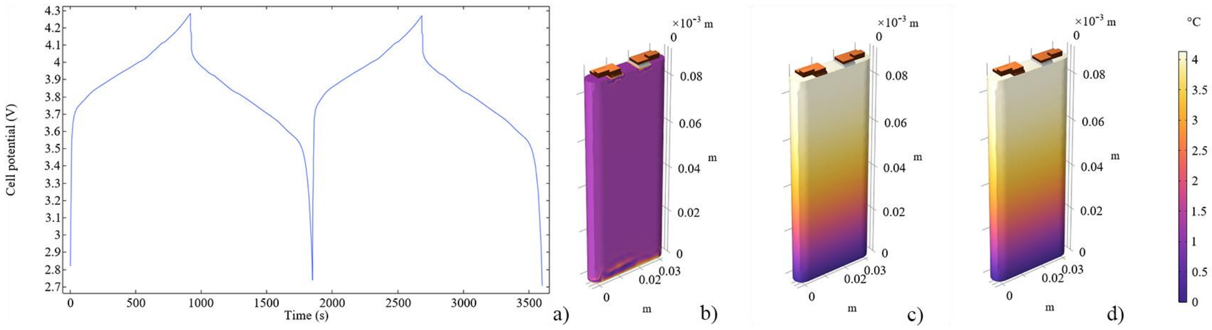

Figure 3: Charge–discharge cycling results at an environmental temperature of $T = 0\,°C$: a) voltage profile, b) battery temperature at the beginning of the 1st cycle, c) battery temperature at the end of the 1st cycle, d) battery temperature at the end of the 2nd cycle.

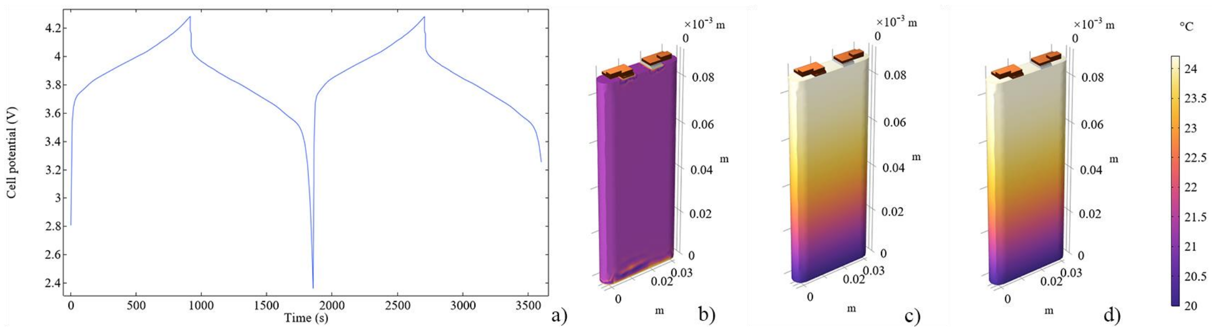

Figure 4: Charge–discharge cycling results at an environmental temperature of $T = 20\,°C$: a) voltage profile, b) battery temperature at the beginning of the 1st cycle, c) battery temperature at the end of the 1st cycle, d) battery temperature at the end of the 2nd cycle.

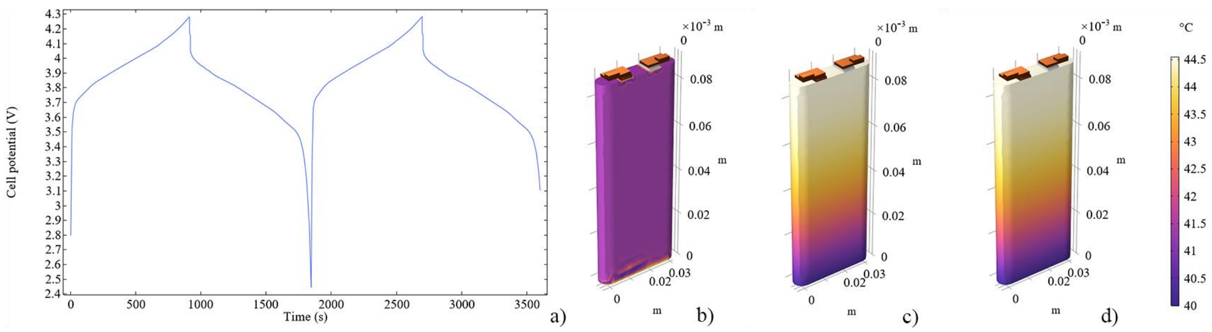

Figure 5: Charge–discharge cycling results at an environmental temperature of $T = 40\,°C$: a) voltage profile, b) battery temperature at the beginning of the 1st cycle, c) battery temperature at the end of the 1st cycle, d) battery temperature at the end of the 2nd cycle.

4.2 Electrical abuse

Electrical abuse primarily refers to scenarios such as overcharging, over-discharging and external short-circuiting during Li-Po battery usage. A simplified overcharging model was established by taking overcharging as an example to study the electrical abuse of batteries. The other internal side reactions were neglected, with the heat generation source being de-fined as micro-short circuits caused by lithium dendrite formation (resulting from lithium plating reactions) penetrating the separator. The total heat generation during overcharging was simulated using a battery cell. The results are shown in Fig. 6. The total heat generation ranged from 13.82 W to 13.95 W through a 3 s simulation. Significant temperature rises were observed in the micro-short circuit region by examining the outer and inner surfaces of the micro-short circuit zone and the cross section of the normal battery cell at the same interval (Fig. 6 d). The outer surface reached a peak temperature of approximately 260 °C after 3 s, and the inner surface attained a peak temperature of 230 °C after 3 s. This finding indicates intense localised reactions and heat generation in the micro-short circuit zone. The high temperature rise on the outer surface is attributed to the thermally insulated boundary condition applied in the simulation, thereby preventing heat exchange with the external environment. Conversely, the low temperature rise on the inner surface resulted from partial heat transfer to adjacent normal battery units through thermal conduction. By contrast, the normal battery cell at the same interval exhibited a maximum temperature rise of 75 °C after 3 s.

The total heat generation of 13.82 W of the battery cell was introduced at 6800 s, whereas the battery voltage stabilised at around 4.35 V by adding thermal events to the lumped model at a 1C rate to simulate micro-short circuit heat generation during overcharging. At $t = 6800$ s, the maximum temperature of the battery occurred at the electrode-current collector interface with a value of 26 °C by simulating the overall temperature change of the battery, and the overall temperature was approximately 22 °C (Fig. 7 b). Cross-sectional analysis at 1/4, 1/2, and 3/4 heights of the battery (Fig. 8 b) showed that the temperature variation in the height direction was not significant, with the internal temperature being high (approximately 23 °C) and the external temperature being low (approximately 21 °C). This result was due to the long simulation charging time, during which battery utilisation and heat exchange with the environment reached equilibrium, thereby resulting in consistent temperature gradients along the heat transfer direction. At $t = 7200$ s, the voltage surged to 4.52 V, marked by an inflection point in the voltage curve (Fig. 7 a). The maximum temperature was approximately 82 °C, and it showed nonuniformity in the height direction of the battery (Fig. 7 c). The cross sections in the height direction indicated that the closer to the positive and negative terminals of the battery, the higher the battery temperature is. As shown in Fig. 8 c, the average temperature at 1/4, 1/2 and 3/4 height was approximately 50, 68 and 78 °C, respectively. The elevated temperatures near the terminals correlate with enhanced electrochemical activity and heat generation rates at the current collector interfaces. After 7200 s, the voltage increased rapidly (Fig. 7 a); at $t = 8000$ s, the battery temperature also increased rapidly, with the maximum value being approximately 105 °C (Fig. 7 d). The cross sections in the height direction of the battery indicated that the average temperature at 1/4, 1/2 and 3/4 height was approximately 59, 85 and 101 °C (Fig. 8 d).

The simulations show that heat generation remains within normal ranges when charging to a battery voltage of 4.35 V, and stable heat exchange with the external environment maintains an overall temperature rise of approximately 2 °C. Beyond 4.35 V, the battery enters an overcharged state. During the initial overcharging phase, the voltage shows no significant change. However, the voltage subsequently rises rapidly as it gradually increases to 4.52 V. This phenomenon is accompanied by a sharp increase in heat generation. At a voltage of 5.65 V, the maximum battery temperature reaches 105 °C. This simulation does not account for side reactions (e.g. electrolyte decomposition and gas generation) that occur internally during overcharging. Consequently, further simulation of temperature evolution under these conditions holds limited practical significance. The results primarily reflect the overall temperature changes in the battery before the onset of overcharge-induced side reactions.

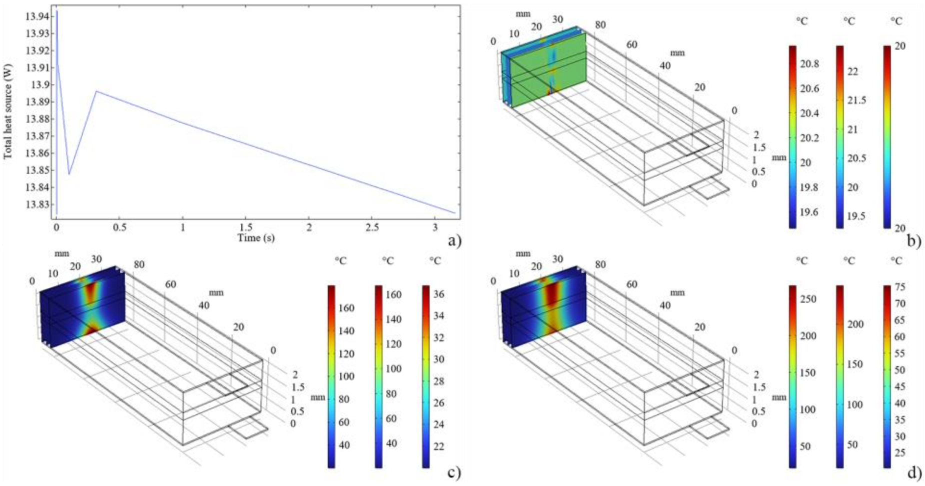

Figure 6: Total heat generation and temperature evolution of the battery cell: a) total heat generation profile, b) temperature at $t = 0$ s, c) temperature at $t = 1.5$ s, d) temperature at $t = 3$ s.

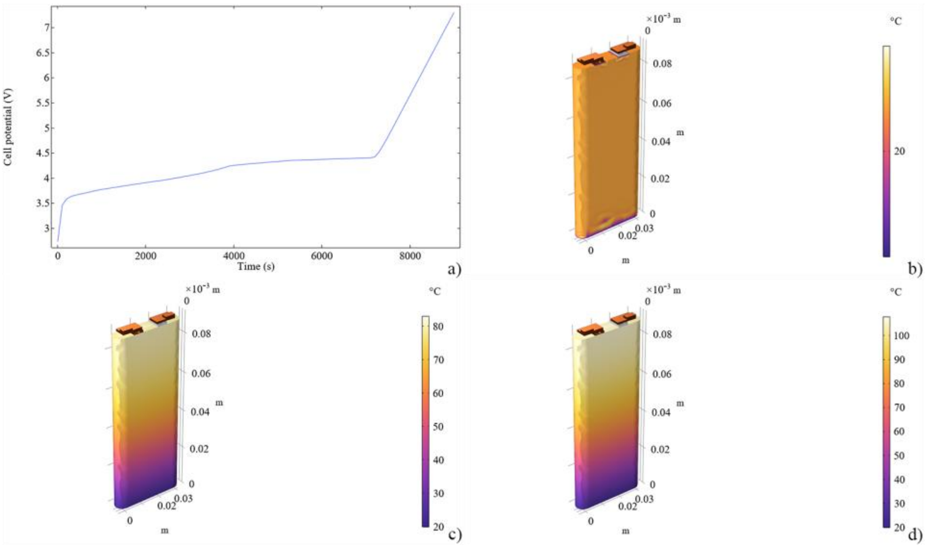

Figure 7: Overcharging results: a) voltage profile, b) battery temperature at $t = 6800$ s, c) battery temperature at $t = 7200$ s, d) battery temperature at $t = 8000$ s.

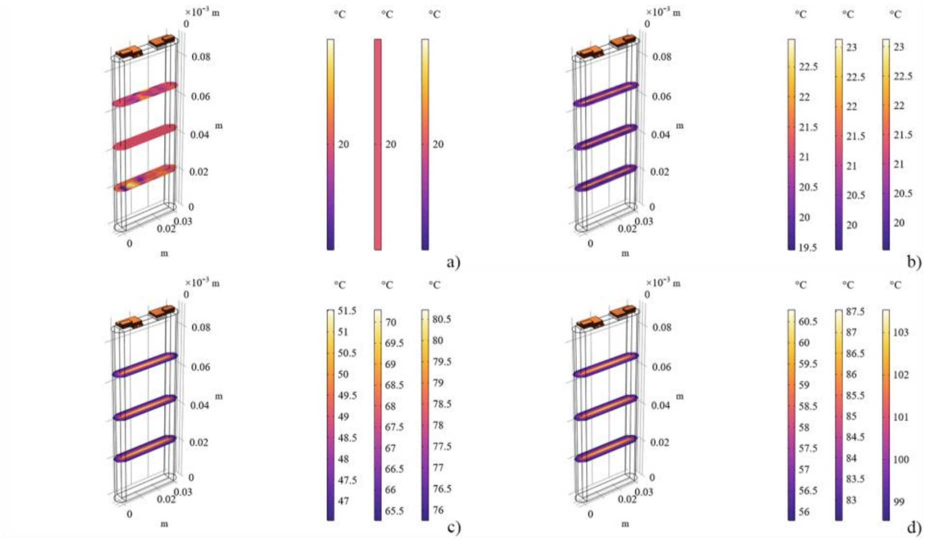

Figure 8: Temperature evolution of the battery during overcharging: a) $t = 0$ s, b) $t = 4000$ s, c) $t = 7200$ s, d) $t = 8000$ s.

4.3 Mechanical abuse

Mechanical abuse refers to the Li-Po battery structural damage caused by external mechanical forces. It leads to internal short circuits, thermal runaway or even explosions. A simplified model was established by taking penetration as a representative case to investigate the mechanical abuse of batteries; however, other internal side reactions were neglected, with the heat generation source being defined as internal short circuits caused by metallic conductor penetration. The total heat generation during mechanical abuse was simulated using a battery cell. The results are shown in Fig. 9. Over a 1 s simulation, the total heat generation ranged from 314.72 W to 315.58 W. Significant temperature rises were observed in the internal short circuit region by examining the outer and inner surfaces of the internal short circuit zone and the cross section of the normal battery cell at the same interval (Fig. 9 d). The outer surface reached a peak temperature of approximately 320 °C after 1 s, and the inner surface attained a peak temperature of 300 °C after 1 s. This observation indicates intense localised reactions and heat generation in the internal short circuit zone. By contrast, the normal battery cell at equivalent intervals exhibited a maximum temperature rise of 22.5 °C after 1 s, with most regions maintaining temperatures around 20 °C. This minimal temperature increase in normal regions suggests negligible heat generation from standard electrochemical reactions, with temperature rises being primarily attributed to the thermal conduction from adjacent short-circuited zones.

The battery was charged to full capacity at $t = 4200$ s with a voltage of 4.27 V by adding thermal events to the lumped model at a 1C rate to simulate heat generation during mechanical penetration. After a resting period, the voltage stabilized at 4.24 V (Fig. 10 a). At $t = 5390$ s, the total heat generation of 315.5 W in the battery cell simulation was introduced, and the penetration depth was set to half the battery thickness. At $t = 5410$s, the maximum temperature of the battery occurred at the puncture location, with a value being approximately 260 °C, by simulating the overall temperature change of the battery (Fig. 10 c). Cross-sectional analysis at 1/4, 1/2, and 3/4 thickness of the battery showed that the temperature in the puncture zone was approximately 230 °C, the temperature at the edge of the puncture zone was approximately 130 °C, and the temperature outside the puncture zone was approximately 47 °C (Fig. 11 c). This gradient arises from intensified electrochemical reactions and high heat generation rates within the penetration zone. At $t = 5420$ s, the battery voltage suddenly dropped, with the maximum temperature being approximately 300 °C (Fig. 10 d). On the three cross sections in the battery thickness direction, the temperature in the puncture zone, at the edge of the puncture zone and outside the puncture zone was around 270, 180 and 85 °C, respectively (Fig. 11 d).

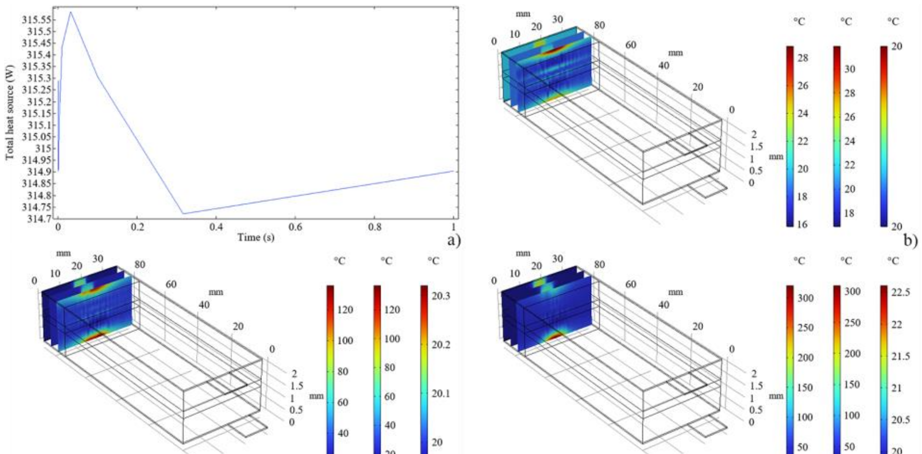

Figure 9: Total heat generation and temperature evolution of the battery cell: a) total heat generation profile, b) temperature at $t = 0$ s, c) temperature at $t = 0.5$ s, d) temperature at $t = 1$ s.

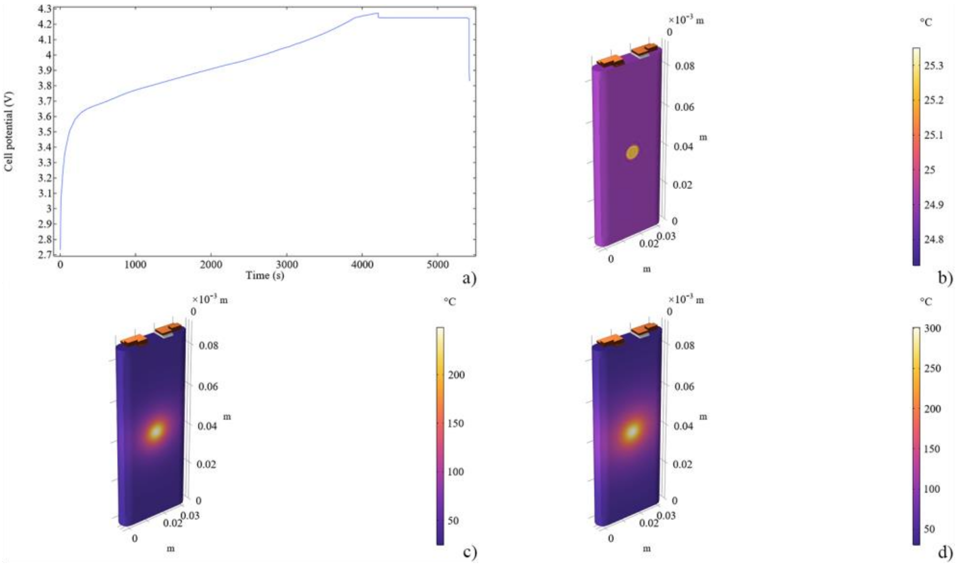

Figure 10: Penetration results: a) voltage profile, b) battery temperature at $t = 5390$ s, c) battery temperature at $t = 5410$ s and d) battery temperature at $t = 5420$ s.

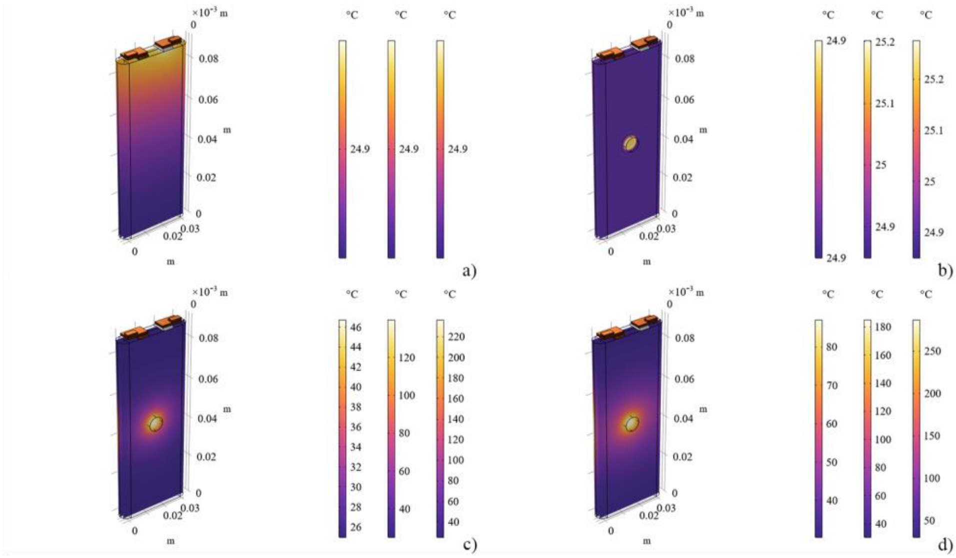

Figure 11: Temperature evolution of the battery during penetration: a) $t = 4200$ s, b) $t = 5390$ s, c) $t = 5410$ s, d) $t = 5420$ s.

The simulations reveal that after mechanical penetration, the battery voltage abruptly drops. This scenario is accompanied by a rapid surge in heat generation, with the maximum temperature exceeding 300 °C within seconds. Given that the model does not account for internal side reactions that may occur postpenetration, the results primarily reflect the overall temperature evolution of the battery before the initiation of penetration-induced side reactions.

5. CONCLUSIONS

With regard to the thermal behaviour of lithium batteries under abnormal ageing conditions, UAV Li-Po batteries were considered the study object. Based on electrochemical theory, numerical simulations were conducted using the lumped battery, lithium-ion battery and solid heat transfer module in COMSOL to analyse temperature evolution under various abuse conditions. The dynamic thermal behaviour of the battery was systematically investigated. The following conclusions were drawn:

(1) Simulations of charge–discharge cycles under different environmental temperatures revealed that high ambient temperatures amplified the battery temperature rise. Elevated environmental temperatures accelerated internal reaction rates and reduced thermal conductivity, thereby leading to increased heat generation and diminished heat dissipation efficiency.

(2) Simulations of temperature evolution under overcharging and penetration conditions revealed that internal short circuits could generate heat, thereby leading to temperature rise. Without accounting for side reactions, the maximum temperature of the overcharged battery reached 105 °C, whereas the penetrated battery attained a peak temperature of 300 °C.

(3) Across all abuse scenarios, the battery model exhibited high temperatures near the positive and negative terminals. This finding is attributed to enhanced electrochemical activity and heat generation rates. Compared with internal regions, the outer surfaces showed elevated temperatures owing to low thermal conductivity at external interfaces, thereby restricting heat dissipation under equivalent heat exchange conditions.

COMSOL can be used to analyse the temperature evolution of UAV Li-Po batteries under abnormal ageing conditions caused by electrode reactions, internal resistance variations and heat transfer mechanisms. A geometric model, established with practical parameters based on abnormal ageing conditions, will have theoretical guiding significance for predicting thermal risks and extending battery life in applications.

For the model established in this study, the parameters were derived from experimental data and literature. However, the simplified internal reaction mechanisms and the complexity of real-world operating conditions collectively restrict the practical applicability of the model to some extent. In the follow-up study, incorporating side reactions and developing models for reaction products and volume changes will significantly enhance the realism and reliability of the simulation results. All the above-mentioned results will constitute the follow-up research direction.

ACKNOWLEDGEMENT

The study was supported by the Scientific Research Team Plan of Zhengzhou University of Aeronautic (No. 24ZHTD02002), the Science and Technology Planning project of Henan Province in China (No. 242102240027).

REFERENCES

[1] Thakur, A. K.; Sathyamurthy, R.; Velraj, R.; Saidur, R.; Pandey, A. K.; Ma, Z.; Singh, P.; Hazra, S. K.; Sharshir, S. W.; Prabakaran, R.; Kim, S. C.; Panchal, S.; Ali, H. M. (2023). A state-of-the art review on advancing battery thermal management systems for fast-charging, *Applied Thermal Engineering*, Vol. 226, Paper 120303, 28 pages, doi:10.1016/j.applthermaleng.2023.120303

[2] Huang, P.; Liu, S.; Ma, J.; Zheng, G.; Li, E.; Wei, M.; Wang, Q.; Bai, Z. (2023). Comprehensive investigation on the durability and safety performances of lithium-ion batteries under slight mechanical deformation, *Journal of Energy Storage*, Vol. 66, Paper 107450, 15 pages, doi:10.1016/j.est.2023.107450

[3] Jantscher, K.; Breitfuß, C.; Miklau, M.; Ismail, K.; Dobusch, P. (2021). Virtual detection of mechanically induced short circuits in a cylindrical lithium-ion battery cell based on finite element simulation, *Batteries*, Vol. 7, No. 4, Paper 79, 26 pages, doi:10.3390/batteries7040079

[4] Li, Y.; Ding, S.; Wang, L.; Wang, W.; Lin, C.; He, X. (2024). On safety of swelled commercial lithium-ion batteries: a study on aging, swelling, and abuse tests, *eTransportation*, Vol. 22, Paper 100368, 13 pages, doi:10.1016/j.etran.2024.100368

[5] Guo, X. Y.; Zeng, Z.; Li, M. X.; Fu, S. (2022). Simulation of aircraft cabin evacuation strategy based on exit flow equilibrium, *International Journal of Simulation Modelling*, Vol. 21, No. 2, 261-272, doi:10.2507/IJSIMM21-2-601

[6] Liu, X.; Guo, B.; He, R.; Jia, P.; Liu, X.; Guo, Y.; Yang, S. (2023). Research on dynamic impact performance of light-UAV battery, *Journal of Mechanical Engineering*, Vol. 59, No. 2, 177-186, doi:10.3901/JME.2023.02.177

[7] Li, N.; Liu, X.; Yu, B.; Li, L.; Xu, J.; Tan, Q. (2021). Study on the environmental adaptability of lithium-ion battery powered UAV under extreme temperature conditions, *Energy*, Vol. 219, Paper 119481, 13 pages, doi:10.1016/j.energy.2020.119481

[8] Finegan, D. P.; Tjaden, B.; Heenan, T. M. M.; Jervis, R.; Di Michiel, M.; Rack, A.; Hinds, G.; Brett, D. J. L.; Shearing, P. R. (2017). Tracking internal temperature and structural dynamics during nail penetration of lithium-ion cells, *Journal of The Electrochemical Society*, Vol. 164, No. 13, A3285-A3291, doi:10.1149/2.1501713jes

[9] Bai, J.; Wang, Z.; Weragoda, D. M.; Tian, G.; Cai, Q. (2024). Thermal runaway of Li-ion batteries caused by hemispherical indentation under different temperatures: battery deformation and fracture, *Journal of Power Sources*, Vol. 621, Paper 235293, 10 pages, doi:10.1016/j.jpowsour.2024.235293

[10] Liu, J.; Duan, Q.; Ma, M.; Zhao, C.; Sun, J.; Wang, Q. (2020). Aging mechanisms and thermal stability of aged commercial 18650 lithium ion battery induced by slight overcharging cycling, *Journal of Power Sources*, Vol. 445, Paper 227263, 9 pages, doi:10.1016/j.jpowsour.2019.227263

[11] Ren, D.; Feng, X.; Liu, L.; Hsu, H.; Lu, L.; Wang, L.; He, X.; Ouyang, M. (2021). Investigating the relationship between internal short circuit and thermal runaway of lithium-ion batteries under thermal abuse condition, *Energy Storage Materials*, Vol. 34, 563-573, doi:10.1016/j.ensm.2020.10.020

[12] Christensen, P. A.; Milojevic, Z.; Wise, M. S.; Ahmeid, M.; Attidekou, P. S.; Mrozik, W.; Dickmann, N. A.; Restuccia, F.; Lambert, S. M.; Das, P. K. (2021).Thermal and mechanical abuse of electric vehicle pouch cell modules, *Applied Thermal Engineering*, Vol. 189, Paper 116623, 16 pages, doi:10.1016/j.applthermaleng.2021.116623

[13] Dong, Y.; Meng, J.; Sun, X.; Zhao, P.; Sun, P.; Zheng, B. (2023). Experimental study on effects of triggering modes on thermal runaway characteristics of lithium-ion battery, *World Electric Vehicle Journal*, Vol. 14, No. 10, Paper 270, 15 pages, doi:10.3390/wevj14100270

[14] Ngandjong, A. C.; Rucci, A.; Maiza, M.; Shukla, G.; Vazquez-Arenas, J.; Franco, A. A. (2017). Multiscale simulation platform linking lithium-ion battery electrode fabrication process with performance at the cell level, *The Journal of Physical Chemistry Letters*, Vol. 8, No. 23, 5966-5972, doi:10.1021/acs.jpclett.7b02647

[15] Chouchane, M.; Rucci, A.; Franco, A. A. (2019). A versatile and efficient voxelization-based meshing algorithm of multiple phases, *ACS Omega*, Vol. 4, No. 6, 11141-11144, doi:10.1021/acsomega.9b01279

[16] Soltani, M.; Vilsen, S. B.; Stroe, A.-I.; Knap, V.; Stroe, D.-I. (2023). Degradation behaviour analysis and end-of-life prediction of lithium titanate oxide batteries, *Journal of Energy Storage*, Vol. 68, Paper 107745, 12 pages, doi:10.1016/j.est.2023.107745

[17] Fuller, T. F.; Doyle, M.; Newman, J. (1994). Simulation and optimization of the dual lithium-ion insertion cell, *Journal of The Electrochemical Society*, Vol. 141, No. 1, 1-10, doi:10.1149/1.2054684

[18] Lee, D.-C.; Kim, C.-W. (2020).Two-way nonlinear mechanical-electrochemical-thermal coupled analysis method to predict thermal runaway of lithium-ion battery cells caused by quasi-static indentation, *Journal of Power Sources*, Vol. 475, Paper 228678, 9 pages, doi:10.1016/j.jpowsour.2020.228678

[19] Fang, W.; Ramadass, P.; Zhang, Z. J. (2014). Study of internal short in a Li-ion cell – II. Numerical investigation using a 3D electrochemical-thermal model, *Journal of Power Sources*, Vol. 248, 1090-1098, doi:10.1016/j.jpowsour.2013.10.004

[20] Kwak, E.; Kim, J.-H.; Hong, S. H.; Oh, K.-Y. (2022). Detailed modeling investigation of thermal runaway pathways of a lithium iron phosphate battery, *International Journal of Energy Research*, Vol. 46, No. 2, 1146-1167, doi:10.1002/er.7235

[21] Savran, E.; Karpat, E.; Karpat, F. (2024). GA and WOA-based optimization for electric powertrain efficiency, *International Journal of Simulation Modelling*, Vol. 23, No. 4, 599-610, doi:10.2507/IJSIMM23-4-699

[22] Fu, S.; Guo, X. Y.; Dong, L. H.; Sheng, K.; Sun, A. (2022). Numerical simulation of migration laws of dense particle flow in pipelines, *International Journal of Simulation Modelling*, Vol. 21, No. 1, 89-100, doi:10.2507/IJSIMM21-1-592